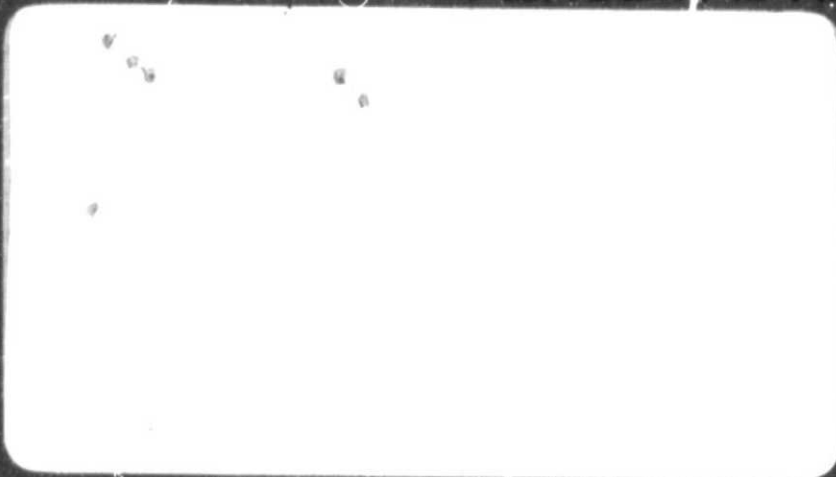


## **General Disclaimer**

### **One or more of the Following Statements may affect this Document**

- This document has been reproduced from the best copy furnished by the organizational source. It is being released in the interest of making available as much information as possible.
- This document may contain data, which exceeds the sheet parameters. It was furnished in this condition by the organizational source and is the best copy available.
- This document may contain tone-on-tone or color graphs, charts and/or pictures, which have been reproduced in black and white.
- This document is paginated as submitted by the original source.
- Portions of this document are not fully legible due to the historical nature of some of the material. However, it is the best reproduction available from the original submission.



(NASA-CR-175858) A MEASUREMENT OF THE  
VIBRATIONAL BAND STRENGTH FOR THE UPSILON  
SUB 3 BAND OF THE HO2 RADICAL Final Report  
(Aerodyne Research, Inc.) 35 p  
HC A03/MF A01

N85-26936

Unclas  
15516

CSCL 07D G3/25

**AERODYNE  
RESEARCH, Inc.**

45 Manning Road  
The Research Center at Manning Park  
Billerica, Massachusetts 01821

A MEASUREMENT OF THE VIBRATIONAL  
BAND STRENGTH FOR THE  $\nu_3$  BAND  
OF THE  $\text{HO}_2$  RADICAL

NASW-3607

Prepared by

Mark S. Zahniser and Alan C. Stanton  
Center for Chemical and Environmental Physics  
Aerodyne Research, Inc.  
45 Manning Road  
Billerica, MA 01821

Final Report  
Contract NASW-3607

Contract Monitor:  
Dr. Robert T. Watson

Prepared for

National Aeronautics and Space Administration  
Environmental Observation Division  
600 Independence Ave. S.W.  
Washington, DC 20546

May 1983

## TABLE OF CONTENTS

<u>Section</u>		<u>Page</u>
	ABSTRACT .....	11
1	INTRODUCTION .....	1-1
2	EXPERIMENTAL DESCRIPTION .....	2-1
	2.1 Flow System .....	2-1
	2.2 Diode Laser Absorption Measurements .....	2-3
	2.3 Measurement of Fluorine Atom Concentrations .....	2-7
3	RESULTS AND DISCUSSION .....	3-1
	3.1 Line Position and Identification .....	3-1
	3.2 Line Strength Determination .....	3-4
4	ACKNOWLEDGMENTS .....	4-1
5	REFERENCES .....	5-1

# ABSTRACT

The HO<sub>2</sub> radicals generated in a discharge-flow system have been observed with tunable diode laser absorption in the P-branch of the  $\nu_3$  vibrational band at 1080 cm<sup>-1</sup>. The observed line positions agree within 2 to 5 x 10<sup>-3</sup> cm<sup>-1</sup> with those calculated from the molecular constants for the  $\nu_3$  band obtained from a previous study using laser magnetic resonance spectroscopy. The band strength has been determined by observing line center absorptions when HO<sub>2</sub> is produced in the reaction  $F + H_2O_2 \rightarrow HO_2 + HF$  ( $k_1$ ) with a measured concentration of atomic fluorine and excess hydrogen peroxide. F-atom concentrations are measured by diode laser absorption of the spin-orbit transition at 404 cm<sup>-1</sup>.

The analysis accounts for HO<sub>2</sub> losses due to the reactions of  $HO_2 + HO_2 \rightarrow H_2O_2 + O_2$  ( $k_3$ ) and  $F + HO_2 \rightarrow HF + O_2$  ( $k_4$ ). The experimental data are consistent with a value of  $k_3 = (1.6 \pm 0.3) \times 10^{-12}$  cm<sup>3</sup>s<sup>-1</sup> and a ratio  $k_4/k_1 = 1.0 \pm 0.4$ . The line strength for the 6<sub>15</sub> + 7<sub>16</sub> F<sub>1</sub> transition is  $2.9 \times 10^{-21}$  cm<sup>2</sup> molecule<sup>-1</sup> cm<sup>-1</sup> which corresponds to a  $\nu_3$  band strength of  $34 \pm 9$  cm<sup>-2</sup> (STP atm)<sup>-1</sup>. This value is a factor of 6 lower than previous ab initio calculations. These results will be useful in assessing the feasibility of atmospheric measurements of HO<sub>2</sub> using infrared absorption techniques.

## 1. INTRODUCTION

The hydroperoxyl radical is an important intermediate species in the chemistry of the upper atmosphere, where it plays an important role in limiting the concentration of stratospheric ozone,<sup>1</sup> and in the lower atmosphere where it participates in the formation of tropospheric ozone.<sup>2</sup> Because of its importance in atmospheric processes and in combustion systems, both the chemical kinetics<sup>3,4</sup> and spectroscopy<sup>5-9</sup> of HO<sub>2</sub> have received intense interest in recent years.

The infrared vibration-rotation spectroscopy of HO<sub>2</sub> is by now well characterized. Measurements of the  $\nu_3$  (O-O stretch) band near 1100 cm<sup>-1</sup> in laser magnetic resonance experiments,<sup>5,6</sup> tunable diode laser absorption measurements<sup>7</sup> of the  $\nu_2$  (bending) band near 1400 cm<sup>-1</sup>, and measurements in the  $\nu_1$  (O-H stretch) band near 3400 cm<sup>-1</sup> using a difference frequency light source<sup>8</sup> have resulted in detailed high resolution analyses of the three fundamental bands of HO<sub>2</sub>. These results, combined with microwave spectroscopy of the ground state,<sup>9</sup> provide a complete set of molecular constants for description of the energy levels and vibration-rotation line positions in the infrared bands.

Although detailed spectroscopic measurements of the HO<sub>2</sub> vibration-rotation energy levels are available, no quantitative measurements of the infrared band strengths have been reported prior to the present study. The laboratory measurement of the band strengths for transient species is difficult compared to such measurements for stable gases since the radicals can be generated only in small concentrations which must be measured by chemical transformations under dynamic or time varying conditions. An approximate absorption cross section for the maximum of the  $\nu_2$  band has been reported in low resolution infrared absorption studies using the molecular

modulation technique by Paukert and Johnston.<sup>10</sup> An ab initio calculation of the intensities for all three fundamental bands has been performed by Komornicki and Jaffe.<sup>11</sup>

In this work, we report the laboratory measurement of the  $\nu_3$  band strength of  $\text{HO}_2$  by using a tunable diode laser to measure the absorption strength of a vibration-rotation line in the P branch near  $1080\text{ cm}^{-1}$ . The  $\text{HO}_2$  is generated in a discharge-flow system by reaction of fluorine atoms with excess  $\text{H}_2\text{O}_2$ ,



The  $\text{HO}_2$  concentration is determined by measuring the F-atom concentration both by chemical titration with  $\text{Cl}_2$  and by tunable diode laser absorption by the F-atom spin-orbit transition near  $404\text{ cm}^{-1}$ . The  $\text{HO}_2$  concentrations in the absorption region are corrected for loss of  $\text{HO}_2$  due to self-reaction, using the second-order decay constant observed in this experiment. The results of this study are important in the development of methods for measurement of absolute concentrations of  $\text{HO}_2$  in the atmosphere or in laboratory kinetics studies.

## 2. EXPERIMENTAL DESCRIPTION

### 2.1 Flow System

The apparatus used in this experiment combines a discharge flow system with a multiple pass absorption cell ("White cell"<sup>12</sup>) aligned so that the optical path is transverse to the direction of flow. Figure 1 is a diagram of this system. This apparatus has been used previously in quantitative measurement of the vibrational band strength of BF using a tunable diode laser.<sup>13</sup> A detailed description of the design of the apparatus is given elsewhere.<sup>14</sup> In the present study, a cylindrical teflon insert with inner diameter of 5.9 cm is used to line the 1 m long flow tube in order to minimize loss of labile species on the flow tube walls. The flow tube is reduced in diameter to 4 cm where the flow enters the IR analysis region. An argon purge flow added to the side arms containing the White cell mirrors provides an effective confinement of the flow tube gases to the central portion of the detection region. This confinement of the flow is an important aspect of the apparatus design because it prevents contact of the labile species with the White cell mirrors or other surfaces in the detection region and also minimizes their traversal time across the path.

Fluorine atoms are produced in a microwave discharge (100 W, 2450 MHz) of F<sub>2</sub> and helium in a 1.0 cm i.d. alumina tube upstream of the main flow tube. The helium flow rate through the discharge is maintained at 34 STP cm<sup>3</sup> s<sup>-1</sup>, and varying flows of F<sub>2</sub> ranging up to 0.34 STP cm<sup>3</sup> s<sup>-1</sup> are used in order to vary the F-atom and HO<sub>2</sub> production. For these conditions where the F<sub>2</sub> is very dilute in the discharge mixture, the percent dissociation of F<sub>2</sub> to form F atoms is found to be essentially independent of F<sub>2</sub> flow rate.

Hydrogen peroxide, obtained as a 90% (by weight) solution from the FMC Corporation, is purified by vacuum distillation such that the original volume is reduced by a factor of 4. Titration with potassium permanganate indicates a resulting purity of greater than 98%. High purity of the H<sub>2</sub>O<sub>2</sub> is important

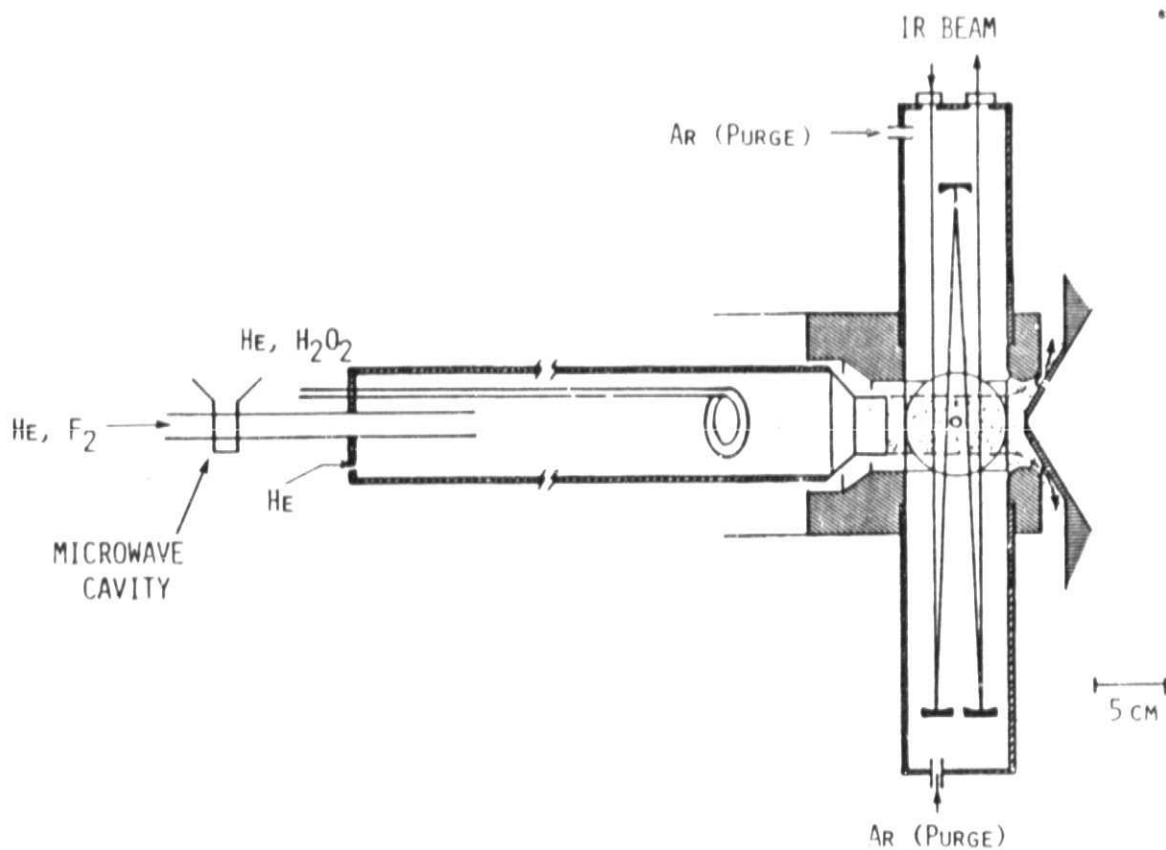


Figure 1. Discharge-flow System with Multiple-pass Absorption Cell. The Ar purge flow in the side arms confines the flow tube gases to the central portion of the absorption path.

because any  $\text{H}_2\text{O}$  impurity could form OH radicals in the reaction  $\text{F} + \text{H}_2\text{O} \rightarrow \text{HF} + \text{OH}$  which could result in incomplete conversion of F to  $\text{HO}_2$ . Purification is particularly important since the  $\text{H}_2\text{O}$  vapor pressure is much greater than that of  $\text{H}_2\text{O}_2$ . The vapor in equilibrium with a 90% by weight solution contains only 50%  $\text{H}_2\text{O}_2$ . The purified  $\text{H}_2\text{O}_2$  is entrained as vapor in a flow of helium ( $5.7 \text{ STP cm}^3 \text{ s}^{-1}$ ) through a pyrex flask containing the liquid  $\text{H}_2\text{O}_2$ . An all glass and teflon system is used to prevent decomposition of  $\text{H}_2\text{O}_2$  between the reservoir and the flow tube. The  $\text{H}_2\text{O}_2$  vapor with its helium carrier flow is added to the flow tube through a movable injector constructed of 6.3 mm o.d. quartz tubing terminating in a loop of tubing with small ( $\sim 0.5 \text{ mm}$  diameter) holes for radial injection to permit rapid mixing with the main flow. Additional helium ( $32 \text{ STP cm}^3 \text{ s}^{-1}$ ) is added to the main flow to provide a linear velocity of  $1180 \text{ cm s}^{-1}$  and a total pressure of 1.85 torr in the flow tube. Flow tube pressure is measured with a capacitance manometer (MKS) and gas flow rates are measured with thermal conductivity-type mass flowmeters (Tylan) calibrated by measuring the change of pressure with time in a known volume. All experiments in this study are conducted at 300 K.

## 2.2 Diode Laser Absorption Measurements

The optical system for the absorption measurements is similar to the multipass absorption system used in previous diode laser measurements in the flow reactor apparatus.<sup>13,14</sup> The tunable diode lasers are mounted in a temperature-controlled closed cycle refrigerator. (Both the lasers and refrigerator are from Spectra-Physics.) The rapidly diverging multimode diode laser emission is collected and collimated by a  $90^\circ$  off-axis paraboloidal reflector with an effective f-number of approximately f/1.2. This radiation is refocused on the entrance slit of a 1-meter focal length monochromator with a 30 groove/mm grating blazed for  $30 \text{ }\mu\text{m}$ . The grating is used in third order for mode selection of the laser used for  $\text{HO}_2$  detection near  $9 \text{ }\mu\text{m}$  and in first order for mode selection of the laser used for fluorine atom detection near  $25 \text{ }\mu\text{m}$ . The single axial mode selected by the monochromator is focused by a pair of off-axis paraboloidal mirrors at the surface of the front spherical mirror of the White cell in the flow reactor analysis region. For these

measurements, the White cell mirrors are adjusted for 40 passes which is a compromise between increased path length and decreased laser signal at the detector due to mirror reflectivity losses. The beam emerging from the White cell is finally focused on an infrared detector. A liquid-helium cooled Ge:Cu photoconductive detector is used for detection near 25  $\mu\text{m}$  in measurement of fluorine atoms and a liquid-nitrogen cooled HgCdTe photoconductive detector is used for detection near 9  $\mu\text{m}$  in measurement of  $\text{HO}_2$ . Both detectors are from Santa Barbara Research Center. A removable, kinematically mounted plane mirror is used for rapid changeover from one detector to the other. Changeover of the entire system from  $\text{HO}_2$  measurement to F atom measurement requires less than five minutes.

The optical system described above is all-reflective and therefore achromatic, which facilitates positioning and alignment of the components with a coaligned helium-neon laser. The helium-neon laser is also used in adjusting the number of passes in the White cell, as determined by counting the spots on the front mirror of the cell. The use of the  $90^\circ$  off-axis paraboloid rather than a lens as the collection optical component is especially convenient in this experiment in that it permits rapid switching from one diode laser to another by a simple translation of the paraboloid. This translation introduces no spherical or chromatic aberration in the system, which would occur if a lens were used in this application. The concern over image quality is appropriate, as we have found that image distortion at the entrance to the White cell can result in interference fringes in the diode laser spectral scans of sufficient amplitude to limit the sensitivity of the absorption measurements. In the present experiment, the amplitude of the residual White cell etalon fringes remaining after careful attention to the optical setup, expressed as a fraction of the laser signal at the detector, is less than  $5 \times 10^{-4}$ .

The absorption signals are detected in either a direct mode, by mechanically chopping the laser radiation at 800 hz and using synchronous detection by a lock-in amplifier (Ithaco Model 393), or as a "second

derivative", by modulating the diode laser current and using synchronous detection at the first harmonic ( $2f$ ) of the modulation frequency  $f$ . The absorption spectra are displayed on an X-Y recorder where the x-axis is driven by the diode laser current which is, to first order, proportional to laser frequency. The line center absorption corresponding to the second derivative signals is determined by calibrating the amplitude of the second derivative signal (peak-to-peak between the primary peak and secondary peaks of the signal) with the fractional absorption at line center measured in direct transmission. The calibration is performed at sufficiently high absorber concentrations to obtain good sensitivity in the direct transmission mode. The advantage of using the second derivative technique is that the baseline is removed, and small fractional absorptions can be detected with greater sensitivity than in the direct transmission mode. One should note that the calibration of second derivative signals as described here applies for a specific current modulation in a particular tuning region of a particular laser mode and assumes that the absorption line shape does not change for the range of conditions under measurement. These conditions are met in the present experiment, where collisional broadening of either the  $\text{HO}_2$  or fluorine atom line is negligible at 2 torr He pressure compared with the room temperature Doppler line width. The calibration also depends on the unattenuated laser intensity  $I_0$  which is monitored at intervals during the measurements.

The laser frequency calibrations are obtained by laser scans of reference calibration gases: OCS in the case of the  $\text{HO}_2$  measurements near  $9\text{ }\mu\text{m}$  and  $\text{CS}_2$  for the F-atom measurements near  $25\text{ }\mu\text{m}$ . The frequency interpolation between reference lines is obtained from the accidental etalon formed in the White cell. The spacing of these interference fringes corresponds to an etalon formed by components with a separation of twice the distance between the White cell mirrors (apparently due to interference between the split halves of the back mirror). For the 50 cm radius of curvature White cell mirrors used in most of the measurements, the fringe separation is  $5.0 \times 10^{-3}\text{ cm}^{-1}$ .

The OCS and CS<sub>2</sub> reference gases are also used to evaluate the laser line width in order to account for possible instrumental broadening effects in analysis of the HO<sub>2</sub> and F-atom absorption spectra. Our previous experience with other diode lasers <sup>13,15</sup> had shown that the finite laser line width can be a significant contribution to the apparent width of a low pressure absorption line, and other measurements have shown that the diode laser line width, particularly for lasers mounted in the closed-cycle refrigerators, often exceeds 10<sup>-3</sup> cm<sup>-1</sup>.<sup>16,17</sup> Scans over low pressure (0.1 torr or less) OCS and CS<sub>2</sub> reference lines with the present lasers produced apparent absorption line widths equal to the room temperature Doppler width of the absorbing species, to the accuracy of the line width measurement, implying negligible instrumental broadening. In the case of the 404 cm<sup>-1</sup> laser (CS<sub>2</sub> measurement), this result implies a laser line width of less than 2 x 10<sup>-4</sup> cm<sup>-1</sup> (6 MHz). Based on these results, no corrections for instrumental broadening are applied in the analysis of the HO<sub>2</sub> or fluorine atom absorption data.

An accurate knowledge of the absorption path length is required for quantitative analysis of the HO<sub>2</sub> absorption data. In the present experiment, effective confinement of the flow in the White cell to the approximately 4 cm diameter core, which corresponds to the flow tube exit diameter, is obtained using the argon purge flow in the arms containing the White cell mirrors (the Ar purge is indicated in Fig. 1). The Ar purge flow rate of 24 STP cm<sup>3</sup>s<sup>-1</sup> is approximately one third that of the main flow through the reaction zone. The actual path length is measured by comparison of the diode laser absorption by a reference OCS line, under flow conditions identical to those used in HO<sub>2</sub> production, with absorption by the same line under static conditions, where the base (single pass) path length is the 50 cm separation of the White cell mirrors. These measurements result in a total path length for the 40 passes of 172 ± 10 cm, corresponding to 4.3 cm/pass.

A point of concern in attempting quantitative absorption measurements with a tunable diode laser is the question of laser mode purity. If more than

one laser mode is transmitted within the bandpass of the monochromator, then scans of the laser mode structure with the monochromator may not reveal the true multiple mode character, and measurements of apparent absorption may be low because a portion of the total intensity is transmitted with no absorption. Indications of impure modes are often revealed in this type of experiment in scans of reference spectra, where absorption features are sometimes repeated or where nominally black absorption lines do not appear black. Neither of these effects occurs in reference scans with the laser modes used here. As noted by Mucha,<sup>18</sup> the "blackness" test is not in itself sufficient to verify mode purity, as very closely spaced satellite modes within the absorption line width may be present. Such a condition should be apparent as an instrumental broadening effect, whereas the absence of significant instrumental broadening in the present experiment supports the assumption of a single monochromatic laser mode. Further support to this conclusion is given by measuring the apparent line strengths of OCS reference lines with the laser used in the HO<sub>2</sub> studies. These measurements are in good agreement with the OCS line strengths tabulated by Maki<sup>19</sup> for lines in the fundamental bands, although discrepancies for line strengths for some of the less well characterized hot bands relative to adjacent fundamental band lines were noted.

### 2.3 Measurement of Fluorine Atom Concentrations

The absolute concentrations of fluorine atoms for the flow conditions used in HO<sub>2</sub> production are determined by a combination of two techniques: chemiluminescent titration with Cl<sub>2</sub> and direct absorption by the F-atom ground state spin-orbit transition near 404 cm<sup>-1</sup>, using a tunable diode laser source. From these measurements, F-atom concentration is correlated with F<sub>2</sub> flow rate through the discharge. The F<sub>2</sub> flow rate is then used as a transfer standard when the hydrogen peroxide is added to the flow system to form HO<sub>2</sub>.

The titration with Cl<sub>2</sub> is a useful technique for measurement of fluorine atom concentrations in the simple mixtures of F and F<sub>2</sub> produced by microwave discharge dissociation of F<sub>2</sub>. The method has been used in several previous

studies<sup>20,21</sup>, and it has been analyzed in detail by Nordine and Rosner.<sup>21</sup> Briefly, the titration is based on the rapid bimolecular reaction of F with Cl<sub>2</sub> to produce Cl atoms:



[ $k_2(300\text{ K}) = 1.1 \times 10^{-10} \text{ cm}^3 \text{ molecule}^{-1} \text{ s}^{-1}$ ]<sup>22</sup>. The Cl-atom production from this reaction is monitored by measurement of the emission arising from the slow three-body recombination of chlorine atoms to form excited Cl<sub>2</sub>, which radiates in the red and near-IR regions through transitions to the ground state. At the titration end point, the Cl<sub>2</sub> and F-atom flow rates are equal, and additional Cl<sub>2</sub> results in no further increase in Cl atom concentration or chemiluminescent intensity. The titration yields a measurement of the fluorine atom concentration at the location where the Cl<sub>2</sub> is injected. The accuracy of this measurement is then dependent on the accuracy of the flow rate measurements and the sharpness of the endpoint.

For the titration, the Cl<sub>2</sub> is injected into the flow tube through the movable quartz injector. The chemiluminescence is monitored downstream in the region coinciding with the absorption path for the diode laser experiments using a Hamamatsu R955 photomultiplier with a red filter with transmission cutoff below 610 nm. The PMT is mounted on the axis orthogonal to the flow and infrared absorption axes. The titration is conducted for several F<sub>2</sub> flow rates and flow tube operating conditions corresponding to the identical flow conditions used in HO<sub>2</sub> production. The calibrated Tylan flowmeters are used to measure flow rates. Titration measurements for different positions of the Cl<sub>2</sub> injector show negligible loss of F-atoms on the teflon flow tube walls for the conditions of this experiment.

The titration technique is found to be quite applicable for the upper range of F<sub>2</sub> flow rates used in the HO<sub>2</sub> experiments. In this range, the endpoints are sharp and can be located to within a 5 to 10% uncertainty in the Cl<sub>2</sub> flow rate. For lower F<sub>2</sub> flow rates, corresponding to fluorine atom

concentrations on the order of or less than  $10^{14} \text{ cm}^{-3}$ , the accuracy of the titration degrades because the endpoint becomes less sharp as the reaction rates decrease. The diode laser absorption technique is used to measure F-atom concentrations in this range. This technique is based on absorption by hyperfine components of the ground state  $^2P_{1/2} + ^2P_{3/2}$  magnetic dipole transition near  $404 \text{ cm}^{-1}$ . The spectroscopy of this transition, including measurements of line positions and line strength, has been established in previous diode laser experiments in this laboratory<sup>23</sup> and by Laguna and Beattie.<sup>24</sup>

Although the  $\text{Cl}_2$  titration technique had been used in the original F-atom diode laser measurements to determine the F-atom absorption line strength,<sup>23</sup> the absorption measurements are recalibrated with the titration in the present experiments. This recalibration is undertaken because improved sensitivity in the diode laser absorption measurements over the original experiments permit calibration over a wider range of fluorine atom concentrations than had been possible originally. Also, the specific line used for the F-atom absorption measurements in this experiment has not been measured in quantitative fashion previously. By recalibration of the F-atom diode laser absorption in this experiment, the  $\text{Cl}_2$  titration is the consistent primary standard for determination of fluorine atom concentrations, and the diode laser technique serves to extend this standard to a lower concentration range where the titration itself is not effective.

The fluorine atom absorption line located at  $403.969 \text{ cm}^{-1}$  is used in the present experiments. This line is the  $F=0 + F=1$  hyperfine component of the transition.<sup>23, 24</sup> Although the  $F=1 + F=2$  line at  $404.177 \text{ cm}^{-1}$  is a factor of 2.5 times stronger than this line, the stronger line falls in a tuning gap of the present diode laser and is therefore not available for measurement. The F-atom line used in these experiments is identified by wavelength calibration from diode laser scans of the low pressure ( $\sim 0.5$  torr)  $\text{CS}_2 \nu_2$  absorption spectrum. The R branch of the  $\text{CS}_2$  fundamental has line spacings of approximately  $0.5 \text{ cm}^{-1}$  in the  $404 \text{ cm}^{-1}$  region, and many other  $\text{CS}_2$  lines from hot bands and isotopic species appear in the same region, providing a rich

source of spectral calibration lines. The CS<sub>2</sub> line positions are taken from high resolution Fourier transform interferometric measurements.<sup>25</sup>

The calibration of the fluorine atom absorption signals using the C<sub>2</sub> titration is shown in Fig. 2, which is a plot of fractional absorption at line center versus F-atom concentration obtained from the titration. This calibration plot is used to determine F-atom concentrations from measured diode laser absorption as a function of discharge F<sub>2</sub> flow rate. From these measurements, the percent F<sub>2</sub> dissociation is determined as a function of F<sub>2</sub> flow rate. For the range of F<sub>2</sub> flow conditions used in HO<sub>2</sub> production, no dependence on F<sub>2</sub> flow rate is found and the measured percent dissociation ( $100 [F]/2 [F_2]$ ) is  $66 \pm 11\%$ . This result is used to correlate fluorine atom concentration with measured F<sub>2</sub> flow rate in analyzing the HO<sub>2</sub> absorption data.

The fluorine absorption calibration data plotted in Fig. 2 may be used to derive a line strength for comparison with the earlier diode laser measurement of the line strength of the stronger F=1 + F=2 line.<sup>23</sup> From the slope of the linear fit to the data in Fig. 2, combined with the absorption path length determination described above, a line center absorption cross section of  $7.2 \pm 0.8 \times 10^{-19} \text{ cm}^2$  is inferred for the F-atom line at room temperature and 2 torr He pressure. The line strength results in Ref. 23 are expressed as the radiative lifetime of the <sup>2</sup>P<sub>1/2</sub> level, averaged over the three transitions due to hyperfine splitting. To derive the radiative lifetime from the present result, one must evaluate the line shape function at line center and account for the thermal distribution of population between the <sup>2</sup>P<sub>1/2</sub> and <sup>2</sup>P<sub>3/2</sub> levels as well as the partitioning of the transition moment among the three allowed transitions. In the case of the line shape, a Voigt profile with negligible instrumental broadening is assumed. The collision broadened component of the line width is taken as  $1.7 \times 10^{-4} \text{ cm}^{-1}$ , from measurements of the room temperature coefficient for broadening by helium.<sup>15</sup> With these assumptions on the line width, the present result leads to a value of 795 s for the <sup>2</sup>P<sub>1/2</sub> radiative lifetime. This result is in excellent agreement with the previous measurement of  $660 \pm 165 \text{ s}$ <sup>23</sup> and the theoretical value of 845 s.<sup>26</sup>

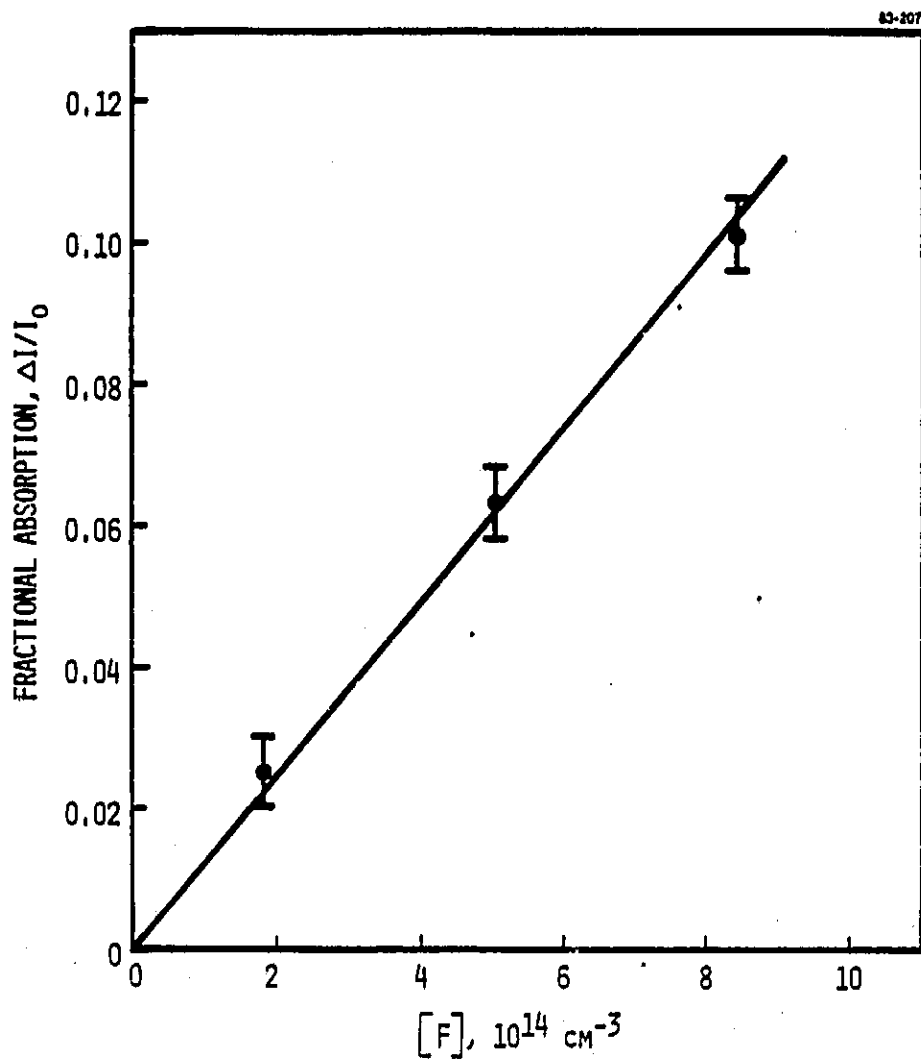


Figure 2. Fractional Absorption at Line Center for the  $^2P_{1/2}(F=0) + ^2P_{3/2}(F=1)$  Transition in Atomic Fluorine. The total path length is 172 cm.

### 3. RESULTS AND DISCUSSION

#### 3.1 Line Position and Identification

The spectrum in Fig. 3 contains four lines of the P-branch of the  $\nu_3$  band of  $\text{HO}_2$ . Predicted line positions of Johns et al.<sup>5</sup>, which are based on laser magnetic resonance data extrapolated to zero field, are also shown along with the transition quantum numbers  $N_K A_K C$ . There is fair agreement between the observed and predicted positions. The calculated line positions are lower in frequency than the observed lines by between  $2$  and  $5 \times 10^{-3} \text{ cm}^{-1}$  with the greatest difference being for the  $6_{15} + 7_{16} F_2$  transition.

The absolute frequency standard for the observed lines is based on the extremely accurate OCS spectral atlas compiled by Maki et al.<sup>19</sup>, which has been invaluable in these experiments. Although the relatively weak OCS reference line shown in Fig. 3 is not included in the Maki et al. compilation, its frequency has been determined from the stronger R75 line of the fundamental  $02^0 0 + 00^0 0$  OCS band as shown in Fig. 4.

The relative frequency standard used in both Figs. 3 and 4 is the interference fringe pattern produced by internal scattering of the laser beam at the back mirrors of the multipass cell. The amount of scattered light and the resultant depth of the interference fringe can be enhanced by changing the entrance angle of the laser beam coming into the cell. The etalon free spectral range is  $1/2d$  where  $d$  is twice the distance between the front and back mirrors of the multipass cell. The spectra in Figs. 3 and 4 were obtained with a mirror spacing of  $40.3 \text{ cm}$  ( $d = 80.6 \text{ cm}$ ) to give a free spectral range of  $6.20 \times 10^{-3} \text{ cm}^{-1}$ . The interference fringes have been maximized in Fig. 4 and are sharp enough to allow relative line positions to be determined to an accuracy of  $\pm 5 \times 10^{-4} \text{ cm}^{-1}$ .

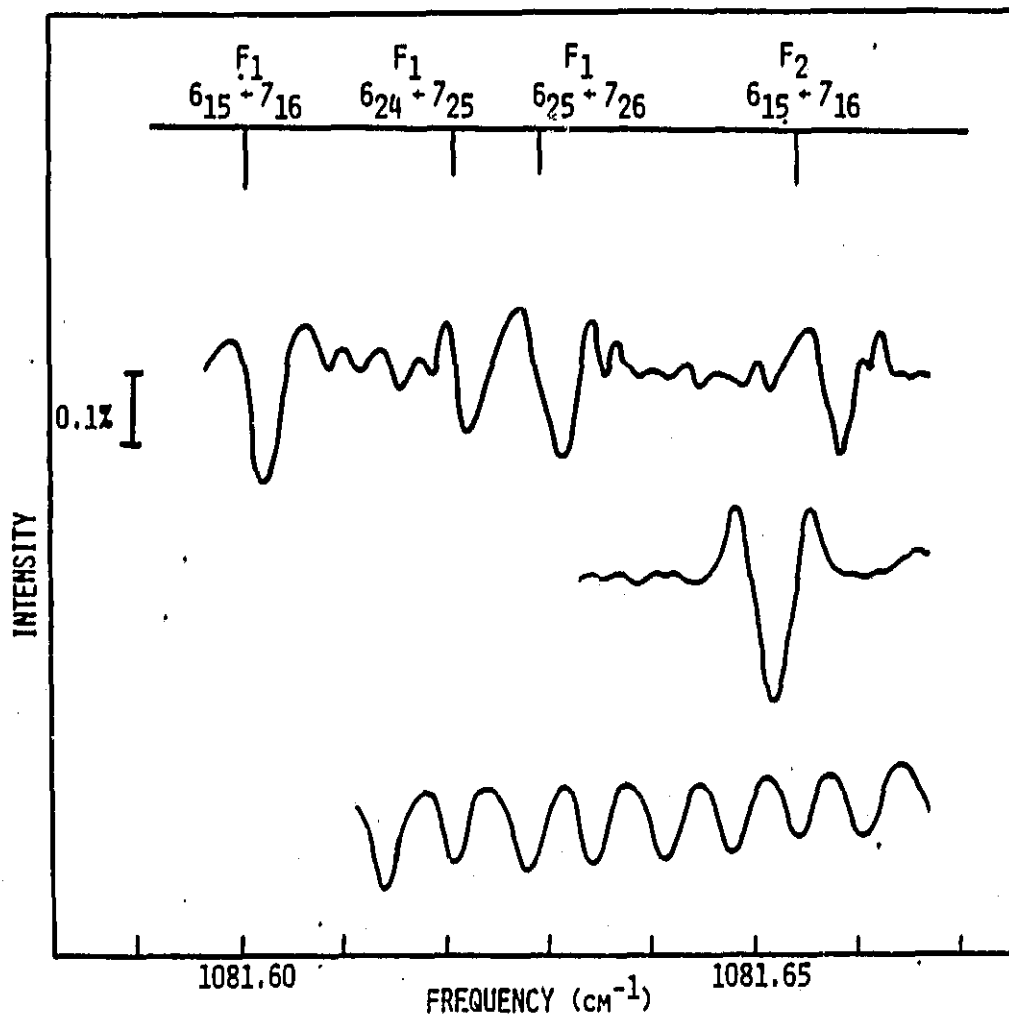


Figure 3. HO<sub>2</sub> Absorption Lines (Second Derivative) from the P-branch of the  $\nu_3$  Band. Predicted positions are from Johns et al. (Ref. 5). The middle trace shows the OCS reference line whose frequency of 1081.6522(5) cm<sup>-1</sup> is determined from Maki et al. (Ref. 19). The frequency scale is determined by the etalon fringes from the multi-pass cell. The fringe spacing is 6.20 x 10<sup>-3</sup> cm<sup>-1</sup>.

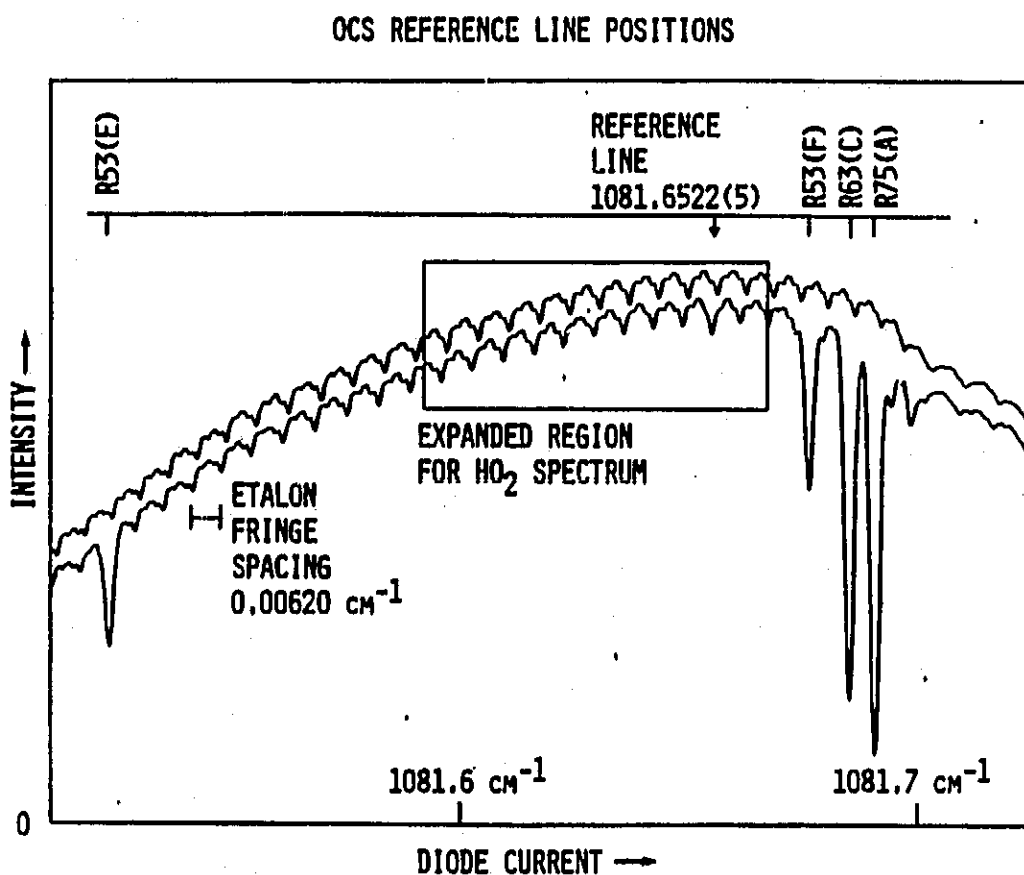


Figure 4. OCS Spectrum Used to Determine Reference Line Frequency for Fig. 3. The upper trace is with the cell evacuated and is offset from the lower trace for clarity. The lower trace is with an OCS pressure of 1.0 torr and a path length of 16m. The calculated line positions and band designations are from Maki et al. (Ref. 19). They are plotted here using the etalon fringes to determine their positions relative to the R75(A) line at  $1081.68878 \text{ cm}^{-1}$ .

The etalon fringes for the spectral scan in Fig. 3 have been minimized so that the weak absorption due to HO<sub>2</sub> is observable. The spectrum is obtained by subtraction of two successive scans, one with and one without the microwave discharge but with all other flow conditions the same. The accuracy of the line position measurements for these HO<sub>2</sub> lines is  $\pm 2 \times 10^{-3} \text{ cm}^{-1}$  and is limited by the low signal-to-noise ratio rather than by the etalon frequency accuracy. The results are summarized in Table 1.

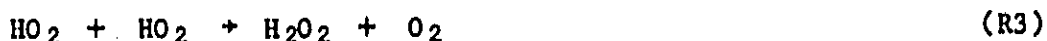
Table 1

Transition $N_{K_a} K_c$	Observed Frequency	Calculated Frequency (Ref. 5)
6 <sub>15</sub> + 7 <sub>16</sub> F <sub>1</sub>	1081.601	1081.603
6 <sub>24</sub> + 7 <sub>25</sub> F <sub>1</sub>	1081.621	1081.623
6 <sub>25</sub> + 7 <sub>26</sub> F <sub>1</sub>	1081.629	1081.632
6 <sub>15</sub> + 7 <sub>16</sub> F <sub>2</sub>	1081.654	1081.659

### 3.2 Line Strength Determination

The fractional absorption at line center,  $A = \Delta I/I_0$ , is measured for the 6<sub>15</sub> + 7<sub>16</sub> F<sub>1</sub> line when excess H<sub>2</sub>O<sub>2</sub> is added to known F-atom concentrations. The movable H<sub>2</sub>O<sub>2</sub> inlet is positioned 15 cm upstream of the absorption path to allow for thorough mixing and for quenching of any vibrationally excited products by collisions with the flow tube walls or with the carrier gas before the detection region. The H<sub>2</sub>O<sub>2</sub> concentration,  $\sim 2 \times 10^{14} \text{ molecules cm}^{-3}$  is in sufficient excess so that the F + H<sub>2</sub>O<sub>2</sub> reaction is essentially complete in the first 2 cm downstream of the injector. The loss of HO<sub>2</sub> on the Teflon walls between its formation region and the detection

point is measured at the lowest HO<sub>2</sub> concentrations and found to be negligible ( $k_w < 3 \text{ s}^{-1}$ ). The loss of HO<sub>2</sub> due to reaction with itself



is non-negligible at higher HO<sub>2</sub> concentrations and must be known in order to relate the HO<sub>2</sub> concentration at the detection point to the initial F-atom concentration. Plots of the reciprocal of the fractional absorption,  $I_0/\Delta I$ , versus H<sub>2</sub>O<sub>2</sub> injector position shown in Fig. 5 are linear over a factor of 5 variation in HO<sub>2</sub> absorption signal and their slopes are independent of initial F-atom concentration for  $2 \times 10^{13} < [\text{F}] < 2 \times 10^{14} \text{ cm}^{-3}$ . Thus, the decay of HO<sub>2</sub> is second order, such that

$$\frac{1}{[\text{HO}_2]_x} = \frac{1}{[\text{HO}_2]_0} + 2k_3 x/\bar{v} \quad (1)$$

where  $[\text{HO}_2]_0$  is the initial HO<sub>2</sub> concentration, produced by  $\text{F} + \text{H}_2\text{O}_2$ ,  $k_3$  is the bimolecular rate constant,  $x$  is the distance along the flow tube and  $\bar{v}$  is the average flow velocity. The slope of the plots in Fig. 5 is  $m = 2k_3/\bar{v}C$  where  $C = A/[\text{HO}_2]$  is the calibration factor relating fractional absorption to HO<sub>2</sub> concentration. If there were complete conversion of F-atoms so that  $[\text{HO}_2]_0 = [\text{F}]_0$ , the HO<sub>2</sub> concentration at the detector corresponding to an observed fractional absorption would be

$$[\text{HO}_2]_{\text{obs}} = [\text{F}]_0 (1 - Am\Delta x) \quad (2)$$

where  $m = 14.5 \pm 1.5 \text{ cm}^{-1}$  is the average of the slopes of the second order plots in Fig. 5 and  $\Delta x$  is the "effective" distance between the H<sub>2</sub>O<sub>2</sub> injector and the detector point. This "effective" distance must account for the mixing and reaction distance for the  $\text{F} + \text{H}_2\text{O}_2$  reaction and for the changes in velocity of the carrier gas as it passes through the narrower neck of the flow tube and into the detection region. The effective "zero" distance for Fig. 5 is determined empirically by comparing the ratios of the absorptions

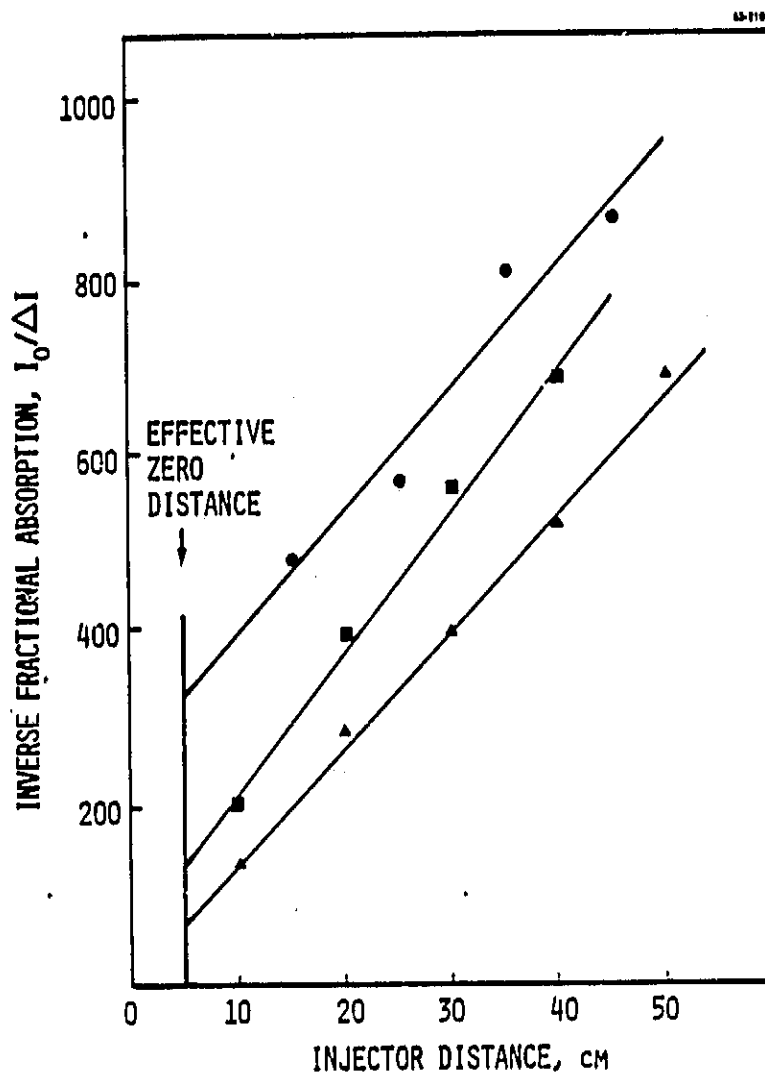


Figure 5. Second Order Decay Plots for  $\text{HO}_2$ . The average flow velocity is  $1060 \text{ cm s}^{-1}$  at  $T=300 \text{ K}$  and  $P=1.8 \text{ torr}$ . The effective zero distance on the x-axis scale is determined by comparing the absorption signal with the initial F-atom concentration.

corresponding to the intercepts to the ratios of the initial HO<sub>2</sub> concentrations which are determined from the measured [F]<sub>0</sub> values as described below. The best match occurs for an effective "zero" distance of 5 cm on the abscissa in Fig. 5 which gives an effective Δx = 10 cm when the injector is fixed at x = 15 cm.

Fractional absorptions are plotted versus [HO<sub>2</sub>]<sub>obs</sub> in Fig. 6. The HO<sub>2</sub> concentrations for the points along the dashed line are calculated from Eq.(2) which accounts for HO<sub>2</sub> removal only by Reaction (3). The curvature of the dashed line at higher [F] indicates that Eq. (2) alone overpredicts [HO<sub>2</sub>] at the detection region and that the conversion efficiency of [F]<sub>0</sub> to [HO<sub>2</sub>]<sub>0</sub> is less than unity. This is most probably due to the reaction



whose rate increases relative to the rate of the F + H<sub>2</sub>O<sub>2</sub> reaction as the F-atom concentration increases relative to [H<sub>2</sub>O<sub>2</sub>]. At low [F] the fraction of [F]<sub>0</sub> which is removed in Reaction 4 is approximated by the ratio of initial rates for Reactions (1) and (4) so that

$$\frac{[HO_2]_0}{[F]_0} \approx 1 - \frac{k_4 [F]_0}{k_1 [H_2O_2]} \quad (3)$$

The points on the solid line in Fig. 6 are corrected for incomplete conversion of [F]<sub>0</sub> to [HO<sub>2</sub>]<sub>0</sub> as described below.

The conversion efficiency of [F]<sub>0</sub> may be calculated by numerically integrating the differential rate equations for Reactions (1), (3), and (4) if their rate constants are known. Although there are published values for k<sub>1</sub> and k<sub>3</sub>, k<sub>4</sub> is unknown. To determine a value for k<sub>4</sub> and the conversion efficiency of F to HO<sub>2</sub>, the flow reactor chemistry is simulated on a computer using these three reactions and the experimental values for flow velocity,

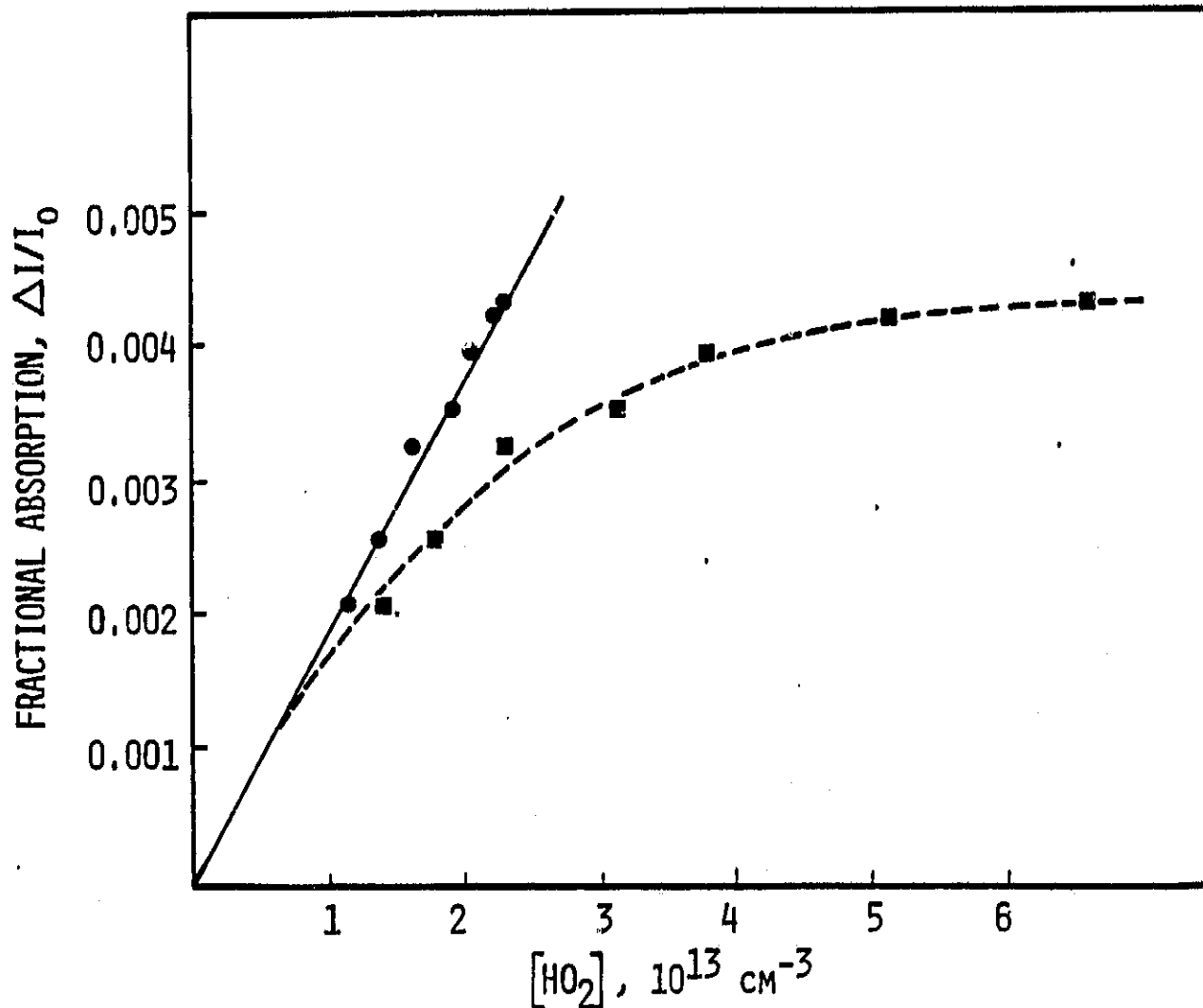


Figure 6. Fractional Absorption at Line Center for the  $615 + 716 \text{ F}_1$  Line of  $\text{HO}_2$  with a Path Length of 172 cm. The  $\text{HO}_2$  concentrations for the points on the dashed line are determined by assuming  $[\text{HO}_2]_0 = [\text{F}]_0$  and correcting only for the second order removal of  $\text{HO}_2$  by Eq. (2) in the 10 cm distance between  $\text{HO}_2$  formation and detection points. The points on the solid line are corrected using Eq. (4) for incomplete conversion of  $[\text{F}]_0$  to  $[\text{HO}_2]_0$  due to the  $\text{F} + \text{HO}_2$  reaction in the initial 2 cm of the reaction zone.

distance, and initial F and H<sub>2</sub>O<sub>2</sub> concentrations. The calculations use values for  $k_1 = 8 \times 10^{-12} \text{ cm}^3 \text{ s}^{-1}$  <sup>27</sup> and  $k_3 = 1.6 \times 10^{-12} \text{ cm}^3 \text{ s}^{-1}$ . <sup>28,29</sup> [HO<sub>2</sub>] is calculated as a function of distance along the flow tube, with a flow velocity of  $1180 \text{ cm s}^{-1}$ . The maximum value for [HO<sub>2</sub>] occurs 2 cm after the starting point. The values for [HO<sub>2</sub>] at  $x = 12 \text{ cm}$  ( $\sim 2 \text{ cm}$  to form HO<sub>2</sub> plus  $10 \text{ cm}$  for decay by Reaction (3)) are calculated for values of  $k_4$  from  $0.5 - 4 \times 10^{-11} \text{ cm}^3 \text{ s}^{-1}$  and are plotted as a function of  $[F]_0$  in Fig. 7 along with the experimentally observed fractional absorptions for the same conditions. The sharp decrease in HO<sub>2</sub> at high  $[F]_0$  occurs when  $[F]_0$  exceeds  $[H_2O_2]$ . As expected, the value for  $[F]_0$  in the model calculations at which this drop occurs is very sensitive to  $[H_2O_2]$  in the model and insensitive to the choice of  $k_4$ . Thus the shape of the high  $[F]_0$  portion of the experimental data is used to refine the value for  $[H_2O_2]$  in the model to  $(2.15 \pm 0.15) \times 10^{14} \text{ cm}^{-3}$  compared to the more approximate experimental value of  $(1.6 \pm 0.8) \times 10^{14} \text{ cm}^{-3}$  determined by the change in pressure in the flow tube with and without H<sub>2</sub>O<sub>2</sub>.

The experimental points are best fitted by a value of  $k_4 = (8 \pm 3) \times 10^{-12} \text{ cm}^3 \text{ s}^{-1}$ . Higher values for  $k_4$  result in a maximum  $[HO_2]_{\text{obs}}$  at too low a value of  $[F]_0$ . The best value for  $k_4$  is dependent on the value of  $k_1$  used in the model. In fact, the fit is most sensitive to the ratio  $k_4/k_1$  rather than to the absolute magnitude of either. The experimental value for  $k_1 = 8 \times 10^{-12} \text{ cm}^3 \text{ s}^{-1}$  from Ref. 27 has a rather large uncertainty and there is other experimental evidence for a value as large as  $5 \times 10^{-11} \text{ cm}^3 \text{ s}^{-1}$ . <sup>30</sup> A higher value for  $k_1$  in the model calculations, when used with a higher value for  $k_4 = k_1 = 4 \times 10^{-11} \text{ cm}^3 \text{ s}^{-1}$ , fits the experimental data equally as well as the fit in Fig. 7 with  $k_4 = k_1 = 8 \times 10^{-12} \text{ cm}^3 \text{ s}^{-1}$ .

The computer calculations of species concentrations as a function of distance verify the observation that both Reactions (1) and (4) go essentially to completion in the first 2 cm, after which only Reaction (3) is important (except for the points with  $[F]_0 > [H_2O_2]$ ). Therefore the computer model is used in the data analysis only to obtain the value for  $\alpha = [HO_2]_0/[F]_0$  at its maximum value at 2 cm downstream of the mixing region. The value for this

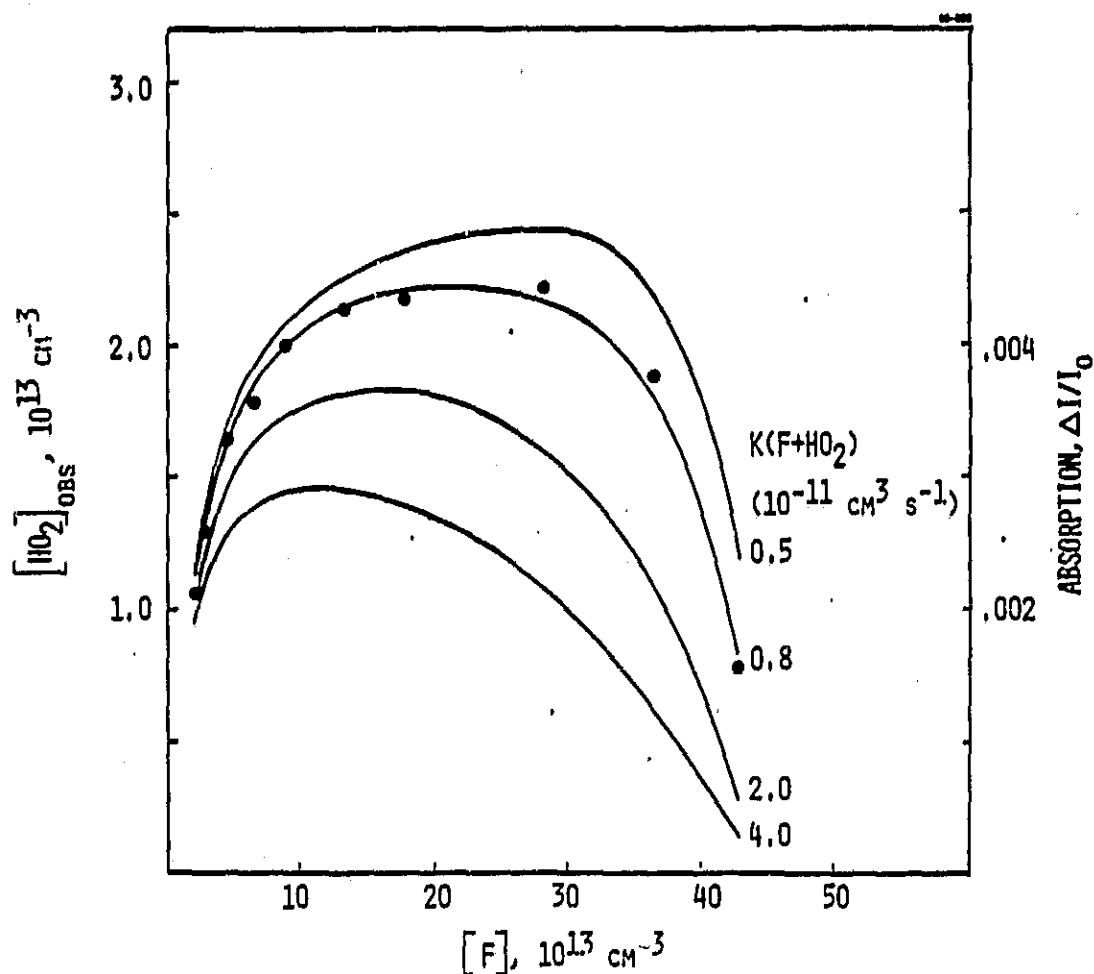


Figure 7. Calculated Values for  $[HO_2]$  at the Detection Region as a Function of Initial  $[F]$  for Different Values of  $k(F+HO_2)$ . The experimentally observed fractional absorptions (right axis) are shown by the solid circles. Flow tube conditions are  $v=1180 \text{ cm s}^{-1}$ ,  $\Delta x=12 \text{ cm}$  and  $[H_2O_2]=2.15 \times 10^{14} \text{ cm}^{-3}$ . The calculated curves use the rate constants  $k(F+H_2O_2)=3 \times 10^{-12} \text{ cm}^3 \text{ s}^{-1}$  and  $k(HO_2+HO_2)=1.6 \times 10^{-12} \text{ cm}^3 \text{ s}^{-1}$ .

ratio is computed using the experimental  $[F]_0$  for each data point.  $[HO_2]_{obs}$  is then obtained by combining this ratio with the second order decay measured rates in Fig. 5 to give

$$[HO_2]_{obs} = [F]_0 \alpha (1 - A_m \Delta x) \quad (4)$$

The experimental data and results of the computer calculations are summarized in Table XI. Values for  $\alpha$  vary from 0.83 to 0.35 for the data points in Figure 6. The  $[HO_2]$  values calculated from Eq. (4) are shown in Fig. 6 with the solid line and give a slope of  $\frac{\Delta I/I}{[HO_2]} = (1.9 \pm 0.5) \times 10^{-16}$  molecules $^{-1}$  cm $^3$ . The overall uncertainty in the calibration factor ( $\pm 25\%$ ) arises from experimental errors in determining  $[F]_0$  ( $\pm 15\%$ ) and  $A$  ( $\pm 15\%$ ) including the calibration of the second derivative signal in terms of fractional absorption. Also contributing to the overall uncertainty are the values for  $m$  and  $\Delta x$  from Fig. 5 which result in a  $\pm 5$  to  $15\%$  (depending on  $[F]_0$ ) uncertainty in determining the correction for  $[HO_2]_{obs}/[HO_2]_0$  due to Reaction (3). The uncertainty in the value for  $k_1$  in the model calculation for  $[HO_2]_0/[F]_0$  results in an uncertainty of  $\pm 10\%$  in the slope of Fig. 6 when  $k_1$  and  $k_4$  are varied by a factor of 5 from  $0.8$  to  $4 \times 10^{-11}$  cm $^3$  s $^{-1}$ .

The line strength at low optical depth may be calculated from

$$S_{line} = \frac{\int (\Delta I/I_0) dv}{[HO_2] \ell} = \frac{\Delta I/I_0}{[HO_2] \ell} \cdot \frac{a}{h} \quad (5)$$

where  $\ell$  is the pathlength (172 cm) and  $a/h = (2.6 \pm 0.3) \times 10^{-3}$  cm $^{-1}$  is the area to height ratio of the absorption line profile determined by tracing the absorption line, taken in the direct transmission mode of operation, with a polar planimeter. The value for  $a/h$  is comparable to that expected for a Doppler broadened line,  $\Delta \nu_D / 2(\ln 2/\pi)^{1/2} = 2.48 \times 10^{-3}$  cm $^{-1}$  at 300 K, which indicates that the instrumental linewidth for this laser mode is small compared to the Doppler width. The line strength for the  $6_{15} + 7_{16}$  F $_1$  transition from Eq. (5) is  $(2.9 \pm 0.7) \times 10^{-21}$  cm $^2$  molecule $^{-1}$  cm $^{-1}$  at 300 K.

Table II Experimental Data for Linestrength Determination

$\frac{[F]_o}{10^{13} \text{ cm}^{-3}}$	$\frac{\Delta I/I_o}{10^{-3}}$	$\frac{[HO_2]_{obs}^a}{[HO_2]_o}$	$\frac{[HO_2]_o^b}{[F]_o}$	$\frac{[HO_2]_{obs}}{10^{13} \text{ cm}^{-3}}$
2.0	2.08	0.70	0.83	1.16
2.8	2.55	0.63	0.78	1.38
4.4	3.25	0.53	0.70	1.63
6.4	3.52	0.49	0.62	1.94
8.8	3.95	0.43	0.54	2.04
13.2	4.22	0.39	0.43	2.21
17.6	4.32	0.37	0.35	2.28
28.0	4.39	0.36	0.21	(2.18) <sup>c</sup>
36.4	3.72	0.46	0.13	(1.82)
42.8	1.54	0.77	0.09	(0.81)

NOTES:

- Calculated from observed second order decay rate in Fig. 5 using Eq. (2) with  $\Delta x = 10 \text{ cm}$  and  $m = 14.5 \text{ cm}^{-1}$ .
- Derived from computer model for Reactions (1), (3), and (4) with  $k_1 = k_4 = 8 \times 10^{-12} \text{ cm}^3 \text{ s}^{-1}$ ,  $k_3 = 1.6 \times 10^{-12} \text{ cm}^3 \text{ s}^{-1}$ ,  $x = 2 \text{ cm}$ ,  $\bar{v} = 1180 \text{ cm s}^{-1}$  and  $[H_2O_2] = 2.15 \times 10^{14} \text{ cm}^{-3}$ .
- $[HO_2]_{obs}$  for points with  $[F]_o > [H_2O_2]$  are calculated from model only with  $x = 12 \text{ cm}$ .

The  $\nu_3$  mode of  $\text{HO}_2$  has a simple parallel band structure ( $\Delta K_a = 0$ ) where the Q-branch intensity is suppressed due to the large ratio of major to minor moments of inertia. Each rotational level is split by the electronic spin of the unpaired electron into  $F_1$  levels with  $J = N + 1/2$  and  $F_2$  levels ( $J = N - 1/2$ ). The line strength for a slightly asymmetric top is related to the band strength by

$$S_{N K_a K_c} = S_{\text{band}} H_{K_a J} \frac{(2J+1) \exp[-F(N, K_a, K_c)/kT]}{2 \sqrt{(\pi/A B C) (kT/hc)^3}} \quad (6)$$

where  $F(N, K_a, K_c)$  is the energy of the lower rotational level. The denominator contains the asymptotic expansion for the rotational partition function for an asymmetric top molecule<sup>31</sup> and an additional factor of 2 to account for the electronic degeneracy of the ground state.  $H_{K_a J}$  is the Honl-London factor<sup>31</sup> for a symmetric top molecule but is applicable in this case for  $\text{HO}_2$  since the asymmetry splitting is so small. For the P-branch ( $\Delta J = -1$ ) this is  $H_{K_a J} = (J^2 - K_a^2)/J(2J+1)$ . Equation (6) gives a ratio of  $S_{\text{band}}/S_{\text{line}} = 436$  for the  $6_{15} + 7_{16}$   $F_1$  transition. The measured line strength then corresponds to a band strength of  $S_{\text{band}} = 34 \pm 9 \text{ cm}^{-2} (\text{STP atm})^{-1}$ .

The line strength to band strength relationship in Eq. (6) is based on the rigid rotor approximation. Deviations from this approximation may occur due to centrifugal distortion and have been observed for the  $\nu_2$  band of  $\text{H}_2\text{S}$ .<sup>32</sup> Such deviations are not expected to be substantial for the  $\nu_3$  band of  $\text{HO}_2$  based on previous spectroscopic evidence. The low resolution spectra of Paukert and Johnston<sup>10</sup> show equal P-branch and R-branch intensities. No anomalous line strength observations are noted by Johns et al.<sup>5</sup> in their LMR study of the  $\nu_3$  band nor by the high resolution studies of the  $\nu_1$  and  $\nu_2$  bands.<sup>7,8</sup> Although these studies were more concerned with line positions than with line strengths, substantial deviations from expected intensities

would have been noted. The four lines observed in this study (Fig. 2) agree with the ratios calculated from Eq. (6), although they are all closely spaced in the P-branch. Relative intensity measurements for lines covering a wider portion of the band are planned for future experiments.

The calibration factor,  $C = (\Delta I/I)/[HO_2]$ , may be used to determine a value for the rate constant  $k_3$  from the slope,  $m$ , of the second order decay plots of Fig. 5:

$$\begin{aligned} k_3 &= m C \bar{v}/2 \\ &= (1.6 \pm 0.3) \times 10^{-12} \text{ molecules}^{-1} \text{ cm}^3 \text{ s}^{-1} \end{aligned} \quad (7)$$

This value is in good agreement with the recent measurements of  $k_3$  at low pressure of Sander et al.<sup>29</sup> who obtained a low pressure limit value of  $(1.6 \pm 0.2) \times 10^{-12} \text{ cm}^3 \text{ s}^{-1}$ , of Thrush and Tyndall,<sup>28</sup>  $(1.6 \pm 0.1) \times 10^{-12}$ , of Simonaitis and Heicklen,<sup>33</sup>  $(1.4 \pm 0.2) \times 10^{-12}$  and of Takacs and Howard<sup>34</sup>,  $(1.5 \pm 0.2) \times 10^{-12}$ . The close agreement of these different studies of  $k_3$  indicates that  $k_3$  is quite well determined at these pressures. Since the absolute number density is required to obtain a second order rate constant, the agreement between the value for  $k_3$  observed in this work and in these other experimental studies is a further confirmation of the band strength determination. In fact the band strength could be determined from just the second order decay plots of Fig. 5 and a literature value for  $k_3$ , without any calibration of  $[F]$ , using only Eq. (7). If one takes  $1.5 \times 10^{-12} \text{ cm}^3 \text{ s}^{-1}$  as the best value for  $k_3$  this method would give a value of  $31 \text{ cm}^{-2} (\text{STP atm})^{-1}$  for the band strength, which is well within the experimental uncertainty of the measurement based on the F-atom concentration.

The band strength may be compared with the previous low resolution experiments of Paukert and Johnston<sup>10</sup> using molecular modulation spectroscopy. They obtain a value of  $5 \times 10^{-20} \text{ cm}^2 \text{ molecule}^{-1}$  for an absorption coefficient at the peak of the R-branch of the  $\nu_2$  band at  $12 \text{ cm}^{-1}$  resolution. Integration over the P and R branches (no significant Q branch

was observed) of the  $\nu_2$  band gives a value of  $\sim 80 \text{ cm}^{-2} (\text{STP atm})^{-1}$  for the  $\nu_2$  band. Combining this with the results of the matrix isolation studies of Smith and Andrews<sup>35</sup> who report relative strengths for the  $\nu_2:\nu_3$  bands of 2:1 gives a value of  $\sim 40 \text{ cm}^{-2} (\text{STP atm})^{-1}$  for the  $\nu_3$  band. The close agreement with this work may be fortuitous in light of the approximate nature of the earlier studies. (Paukert and Johnston<sup>10</sup> claim an accuracy only within a factor of two for their absorption measurement.)

The result of this study may also be compared with the ab initio calculations of Komornicki and Jaffe<sup>11</sup> who calculate a value of  $207 \text{ cm}^{-2} (\text{STP atm})^{-1}$  for the  $\nu_3$  band and  $237 \text{ cm}^{-2} (\text{STP atm})^{-1}$  for the  $\nu_2$  band. The value for the  $\nu_3$  band is larger by a factor of six than the experimental result and the ratio of strengths for  $\nu_2$  to  $\nu_3$  bands is nearly unity compared to the 2:1 ratio observed in the matrix isolation studies.<sup>35</sup> Such a large disagreement between theory and experiment for  $\text{HO}_2$  is somewhat surprising since good agreement has been obtained for the bands of  $\text{HOC}\ell$  and for  $\text{C}\ell\text{O}$  using the same calculational method.<sup>11</sup>

The relatively low value for the band strength makes atmospheric measurements of  $\text{HO}_2$  using the  $\nu_3$  band more difficult than previously anticipated and may make other bands more attractive as alternatives. Although the  $\nu_2$  band at  $1390 \text{ cm}^{-1}$  may be more intense, its use in an atmospheric measurement is complicated by  $\text{CH}_4$  and  $\text{N}_2\text{O}$  lines in the same region. Similarly, the  $\nu_1$  band at  $3440 \text{ cm}^{-1}$  is in a region of  $\text{H}_2\text{O}$  absorption. In both regions, however, there are likely to be transmission "windows" at high resolution which could allow specific  $\text{HO}_2$  lines to be used. In view of the discrepancy between the present result for the  $\nu_3$  band strength and the theoretical calculations, quantitative assessment of techniques based on absorption in the  $\nu_1$  or  $\nu_2$  bands of  $\text{HO}_2$  requires the experimental measurement of these two band strengths as well.

#### 4. ACKNOWLEDGMENTS

We are indebted to Dr. A.G. Maki of the National Bureau of Standards for providing OCS reference line positions prior to publication. We also thank Drs. J. Wormhoudt, C.E. Kolb, J.A. Silver, and F. Kaufman for helpful discussions. The technical assistance of W.E. Goodwin is gratefully acknowledged. This work has been supported by the Chemical Manufacturers Association under contract FC 81-355 and by NASA under contract NASW-3607.

## 5. REFERENCES

1. J.A. Logan, M.J. Prather, S.C. Wofsy, and M.B. McElroy, Phil. Trans. R. Soc. London A 290, 187 (1978).
2. J.A. Logan, M.J. Prather, S.C. Wofsy, and M.B. McElroy, J. Geophys. Res. 86, 7210 (1981).
3. "Chemical Kinetic and Photochemical Data for Use in Stratospheric Modelling", JPL Publication 81-3, Jet Propulsion Laboratory (Pasadena CA, 1981).
4. F. Kaufman, Ann. Rev. Phys. Chem. 30, 411 (1979).
5. J.W.C. Johns, A.R.W. McKellar, and M. Riggin, J. Chem. Phys. 68, 3957 (1978).
6. A.R.W. McKellar, Faraday Discuss. Chem. Soc. 71, 63 (1981).
7. K. Nagai, Y. Endo, and E. Hirota, J. Molec. Spectrosc. 89, 520 (1981).
8. C. Yamada, Y. Endo, and E. Hirota, J. Chem. Phys. 78, 4379 (1983).
9. A. Charo and F.C. DeLucia, J. Molec. Spectrosc. 94, 426 (1982).
10. T.T. Paukert and H.S. Johnston, J. Chem. Phys. 56, 2824 (1972).
11. A. Komornicki and R.L. Jaffe, J. Chem. Phys. 71, 2150 (1979).
12. J.U. White, J. Opt. Soc. Am. 32, 285 (1942).
13. M.S. Zahniser and M.E. Gersh, J. Chem. Phys. 75, 52 (1981).
14. M.E. Gersh, J.A. Silver, M.S. Zahniser, C.E. Kolb, R.G. Brown, C.M. Gozewski, S. Kallelis, and J.C. Wormhoudt, Rev. Sci. Instrum. 52, 1213 (1981).
15. A.C. Stanton, J.C. Wormhoudt, and J.W. Duff, Proceedings of the 6th International Conference on Spectral Line Shapes, Walter de Gruyter, (Berlin, 1983), pp. 515-529.
16. J. Reid and A.R.W. McKellar, Phys. Rev. A 18, 224 (1978).
17. J. Reid, D.T. Cassidy, and R.T. Menzies, Appl. Opt. 21, 3961 (1982).
18. J.A. Mucha, Appl. Spectrosc. 36, 141 (1982).
19. A. Maki and J.S. Wells, J. Chem. Phys. Ref. Data, 1983, to be published.

20. P.S. Ganguli and M. Kaufman, Chem. Phys. Lett. 25, 221 (1974).
21. P.C. Nordine and D.E. Rosner, J. Chem. Soc. Faraday Trans. 1 72, 1526 (1976).
22. M.A.A. Clyne, D.J. McKenney, and R.F. Walker, Can. J. Chem. 51, 3596 (1973).
23. A.C. Stanton and C.E. Kolb, J. Chem. Phys. 72, 6637 (1980).
24. G.A. Laguna and W.H. Beattie, Chem. Phys. Lett. 88, 439 (1982).
25. K. Jolma and J. Kauppinen, J. Molec. Spectrosc. 82, 214 (1980).
26. A.M. Naqvi, Thesis, Harvard University (1952).
27. D.J. Smith, D.W. Setser, K.C. Kim, and D.J. Bogan, J. Phys. Chem. 81, 898 (1977).
28. B.A. Thrush and G.S. Tyndall, Chem. Phys. Lett. 92, 232 (1982).
29. S.P. Sander, M. Peterson, R.T. Watson, and R. Patrick, J. Phys. Chem. 86, 1236 (1982).
30. F. Temps and H.G. Wagner, Ber. Bunsenges, 86, 119 (1982).
31. G. Herzberg, Molecular Spectra and Molecular Structure, Vol. II, Infrared and Raman Spectra of Polyatomic Molecules, van Nostrand (New York, 1945), p. 506, pp. 421-422.
32. L.L. Strow, J. Quant. Spectrosc. Radiat. Transfer 29, 395 (1983).
33. R. Simonaitis and J. Heicklen, J. Phys. Chem. 86, 3416 (1982).
34. G.A. Takacs, private communication (1983).
35. D.W. Smith and L. Andrews, J. Chem. Phys. 60, 81 (1974).